Combustion, Explosion, and Shock Waves, Vol. 40, No. 5, pp. 591–596, 2004

Radiographic Study of the Evolution Material of the Density Profile behind the Front of a Divergent Shock Wave in an Explosive

K. N. Panov[1] and V. A. Komrachkov[1]

UDC 662.215.5

Translated from *Fizika Goreniya i Vzryva*, Vol. 40, No. 5, pp. 102–108, September–October, 2004.
Original article submitted July 17, 2003; revision submitted December 3, 2003.

The evolution of the material density profile behind the front of a divergent initiating shock wave in HMX and RDX based explosives in the transitional regime of explosive transformation was studied using flash radiography. The explosives were loaded by a divergent shock wave through a Plexiglas layer of varied thickness. Distinctive features were found in the evolution of the density profile behind the front of a divergent initiating shock wave that did not become a detonation wave and behind the front of an initiating shock wave that became a detonation wave.

Key words: explosive, initiating shock wave, detonation, flash radiography, material-density distribution.

INTRODUCTION

For studies of the initiation of detonation of heterogeneous explosives (HEs) by a shock wave (SW), along with data on the parameters of the shock front in the transitional region, information on the processes behind the shock front is important. Recently, explosive transformations have been studied using electromagnetic and Manganin gauges, which are in contact to the tested material and can influence the formation of a detonation regime. In this respect, flash radiography has obvious advantages in studies of explosive transformations. This method allows one to visualize the process and to determine the material-density distribution behind the initiating SW front and in other characteristic zones of the loaded HE: the starting HE; the shock compressed HE; and the zone of dispersion of the explosion products.

This paper describes a flash radiographic study of the evolution of the material-density profile behind the front of a divergent initiating SW in HMX and RDX based HEs in the transitional regime of the explosive transformation.

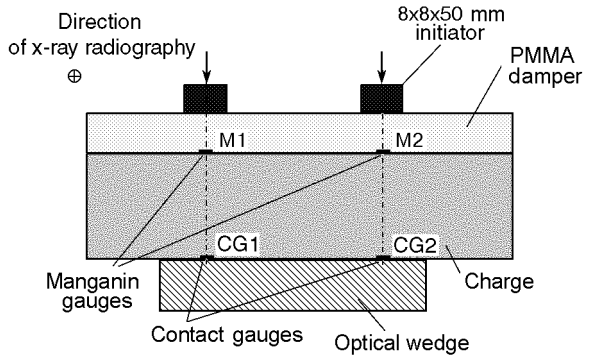

Fig. 1. Diagram of experimental assembly.

EXPERIMENTS

The experiments were performed on a 2ÉRIDAN-3radiographic facility with a soft radiation spectrum with a boundary energy $E_\gamma \approx 0.75$ MeV and a radiation pulse duration $\Delta t \approx 0.3$ μsec. Figure 1 gives a diagram of the experimental assembly. The loading system is described in [1, 2]. The tested HE sample was set off by two extended priming charges based on PETN through a damping Plexiglas layer. The initiating SW pressure was varied by changing

[1]Institute of Experimental Physics, Institute of Experimental Gas Dynamics and Physics of Explosion, Russian Federal Nuclear Center, Sarov 607190; root@gdd.vniief.ru.

the thickness of the damping layer. The loading-pulse profile was recorded by M1 and M2 Manganin gauges placed between the damper and the tested charge. The primers operated at different times, which allowed us to take two phases of the process in single-frame shooting. The exact time when the HE began to be loaded by each of the primers was determined from the moments of operation of the Manganin gauges. The moments the shock (detonation) wave arrived at the bottom surface of the charge under each primer were recorded by contact gauges (CG1 and CG2).

The tested charge had dimensions of 120 $\times$ 20 (30) mm and a thickness in the direction of radiography of 45 mm. The tested sample was placed on a cartridge of the same explosive composition of 60 mm diameter, which served as an optical wedge. It was used to compare the photographic density of the x-ray film D and the optical distance of the radiographed object $z = \rho L$, where ρ is the density and L is the dimension of the sample in the direction of radiography.

One of the first measurements of compression of an inert material at the SW front using flash radiography was performed by Schall in 1950 [3]. The examined object (10$\times$10 mm bar) was radiographed together with a stepped reference sample made of the same material. He studied the compression of light materials (Mg and Al) at the SW front in metallic bars adjoining a HE charge of equal cross section.

Recently, there have been numerous studies of the state of materials behind the front of shock (detonation) waves using radiations of different types [4–7]. They were concerned mostly with the problem of determining the material density behind the front of a detonation wave (DW) or an initiating SW.

RESULTS OF EXPERIMENTS AND CALCULATIONS OF DENSITY DISTRIBUTION USING EXPERIMENTAL DATA

The loading-pulse profile was measured with a Manganin gauge. The sensing element of the gauge was a Manganin foil strip with dimensions of 8$\times$0.5 mm and a thickness of 0.03 mm. In the experiments, the gauges were placed on Fluoroplastic insulation 0.015 mm thick. In the determination of the loading profile in the initiating cylindrical SW, the sensing element of the gauge was located along the line of initiation. The gauge design and the location of its sensing element relative to the initiating SW front lead to minimum stretching of the gauge and reduce the effect of this factor on the pressure measurement.

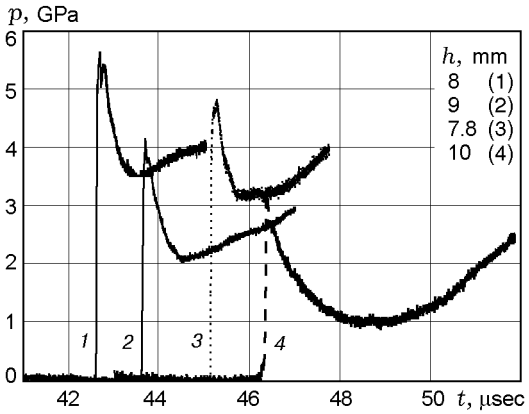

Fig. 2. Loading-pressure profiles for various damper thicknesses: curves 1 and 2 refer to HMX based HE and curves 3 and 4 refer to RDX based HE.

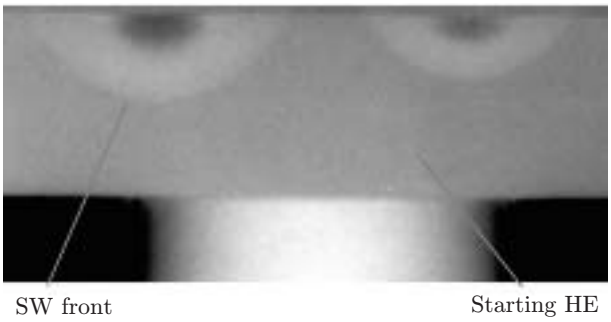

Fig. 3. Radiograph of an experiment with an HMX based HE ($h = 9$ mm; detonation failure).

Figure 2 gives loading-pressure profiles for various damper thicknesses h and different HEs. The loading-pressure profiles are characteristic of a nonstationary initiating SW. Behind the front, the curves of $p(t)$ shows a pressure increase, most likely due to the beginning of HE decomposition.

Figure 3 gives a radiograph of an experiment with an HMX based HE in which transition from the shock wave to a detonation wave was not detected at the moment of radiography. In the radiograph, one can see a region of undisturbed HE, the SW fronts which traveled different distances at the moment of radiography, and a region of compressed HE behind the SW front (the lighter zone on the radiograph). Behind the light zone on the photograph there is a darker region. The photographic density of the x-ray film in this zone is higher than that on the image of the starting HE, which can indicate HE decomposition.

Figure 4 gives a radiograph of an experiment in which a transitional regime of the explosive transformation of an RDX based HE was detected at the moment of radiography. The SW front becomes a DW front.

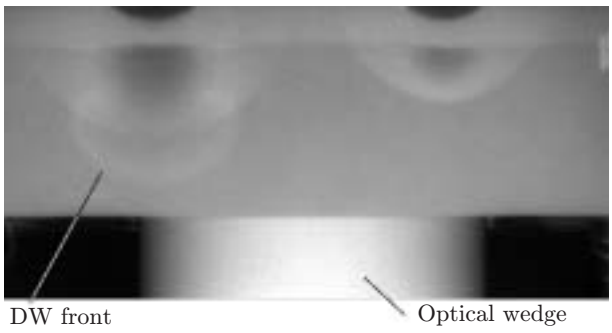

Fig. 4. Radiograph of an experiment with an RDX based HE ($h = 7.8$ mm; transition to detonation).

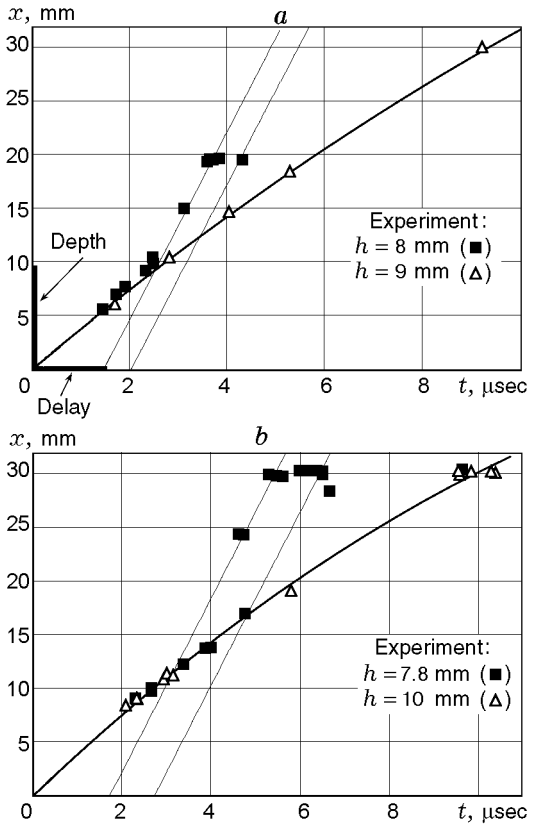

Fig. 5. x–t Diagram of propagation of SW (DW) fronts: the thick solid curve is the total dependence plotted from the results of all experiments using the least-squares method.

Figure 5 gives x–t diagrams of the propagation of SW and DW fronts with various damper thicknesses for different HEs. The resulting dependence shows that for the HMX based HE with a damper thickness $h = 9$ mm, which corresponds to a maximum pressure at the front $p_{\max} \approx 4.0$ GPa, the explosive transformation does not become a detonation. The velocity of the SW front decreases as the SW propagates over the HE.

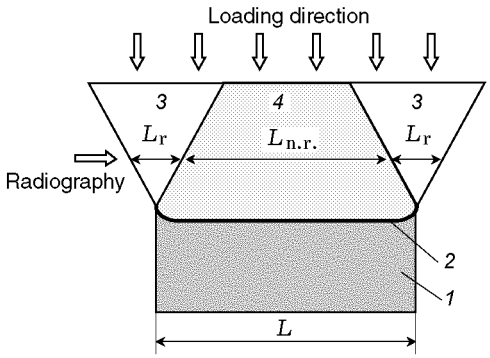

Fig. 6. Loading diagram: 1) unloaded HE; 2) SW (DW) front; 3) rarefaction region; 4) region not encompassed by rarefaction.

For $h = 8$ mm (and, accordingly, $p_{\max} \approx 5.5$ GPa), transition from the SW to a DW is detected. Two straight lines bounding the zone of transition from the SW to a DW are drawn through the points of the x–t diagram corresponding to the moments of exit of the waves from the sample. At a depth of ≈9.5–12 mm (the point of inflection in the x–t diagram), the SW front became a DW front. The delay of detonation initiation specified by the point of intersection of the detonation straight line of the x–t diagram with the time axis t [8] was ≈1.45–2.0 μsec.

For the RDX based HE with $h = 10$ mm (and, accordingly, $p_{\max} \approx 3.2$ GPa), the explosive transformation does not become a detonation. The velocity of the SW front decreases as the SW propagates over the HE.

For $h = 7.8$ mm ($p_{\max} \approx 4.7$ GPa), transition from the SW to detonation was detected. At a depth of ≈11.5–17 mm, the SW front became a DW front. The delay of detonation initiation was ≈1.7–2.6 μsec.

The method of determining the density profile is based on the relation between the photographic density of the x-ray film D and the optical distance of the radiographed object $z = \rho L$. A microphotogram $D(x)$ is plotted in an isolated direction on the image of the studied object. A curve of $z(x)$ — the optical-distance distribution along the coordinate — was plotted using the reference dependence $D(z)$ obtained by radiography of the optical wedge. The density distribution $\rho(x)$ was found from the relation $\rho(x) = z(x)/L$. In this relation, the effect of rarefaction on the accuracy of the density distribution is not included in explicit form.

Let us estimate the effect of the dispersion of the material from the end surfaces on the determination of the density profile. For this, we revert to Fig. 6. It is evident from the figure that behind the initiating SW front, the x-ray is attenuated when passing the zones of the

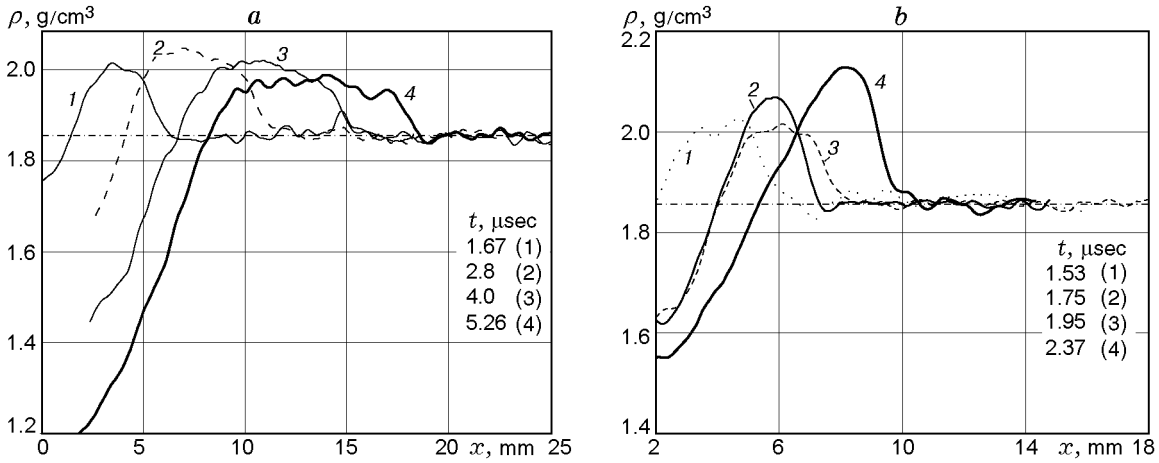

Fig. 7. Material-density distribution behind the SW front for the HMX based HE: (a) $h = 9$ mm; detonation failure' (b) $h = 8$ mm; transition to detonation; the dot-and-dashed curve refers to the initial density.

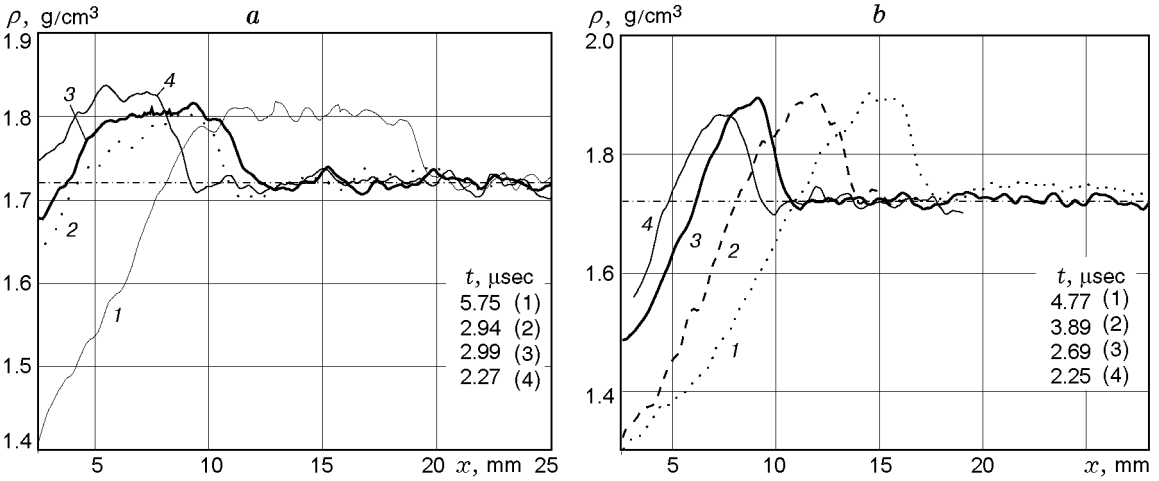

Fig. 8. Material-density distribution behind the SW front for the RDX based HE: (a) $h = 10$ mm; detonation failure; (b) $h = 7.8$ mm; transition to detonation; the dot-and-dashed curve refers to the initial density.

material encompassed by rarefaction (regions 3) and the region of the material that are not encompassed by rarefaction (region 4). In regions 3, the density varies from the value $\rho_{\text{n.r.}}$ (the required quantity) on the boundary of region 4 to zero, i.e., there is a certain lengthwise distribution of the density. Along the x-ray, it is not important to know the functional form of this distribution (since the attenuation of the radiation depends on the mean density on the length L_{r}), which in a linear approximation can be defined as $\rho_{\text{r}} = \rho_{\text{n.r.}}/2$.

The optical distance z behind the SW front is given by

$$z = 2L_{\text{r}}\rho_{\text{r}} + L_{\text{n.r.}}\rho_{\text{n.r.}}, \tag{1}$$

where L_{r} is the dimension of the rarefaction region, ρ_{r} is the density in this region, $L_{\text{n.r.}}$ and $\rho_{\text{n.r.}}$ are the same quantities for the zone that is not encompassed by rarefaction. Substituting $\rho_{\text{r}} = \rho_{\text{n.r.}}/2$ into Eq. (1), we obtain

$$z = \rho_{\text{n.r.}}(L_{\text{r}} + L_{\text{n.r.}}). \tag{2}$$

Assuming that the dispersion of the material in regions 3 (see Fig. 6) is symmetric, we have

$$L = L_{\text{r}} + L_{\text{n.r.}}. \tag{3}$$

Substituting Eq. (3) into Eq. (2), we obtain

$$z = \rho_{\text{n.r.}}L, \tag{4}$$

whence

$$\rho_{\text{n.r.}} = z/L. \tag{5}$$

Thus, the use of the relation $\rho(x) = z(x)/L$ means that the density is determined by a change in the magnitude of radiation attenuation at each point compared to the magnitude of attenuation in the undisturbed zone of the sample.

In practice (with rarefaction waves from the end surfaces), the same approach implies that the radiation attenuation on a path of length $2L_{\mathrm{r}} + L_{\mathrm{n.r.}}$ with the corresponding densities is equivalent to the radiation attenuation on the length L with the required density $\rho_{\mathrm{n.r.}}$. In [4, 5], the same approach was used to determine the dependence $\rho(t)$.

Figure 7 gives density profiles determined along the line of loading of the HMX based HE with $h = 9$ and 8 mm. The coordinate $x = 0$ corresponds to the loaded surface of the HE. The times indicated in the diagram are reckoned from the moment of entry of the initiating SW into the HE charge. From Fig. 7 it is evident that in the case of detonation failure, the compressed material layer increases during SW propagation; the thickness of this layer is determined as the width of the density profile at half-height. In the compression region, the material density behind the SW front changes insignificantly and is $\approx$2.0 g/cm^3.

For transition from the SW to a DW, the obtained relations differ from the data of experiments in which detonation was absent (see Fig. 7). In the process of SW propagation, the material density behind the front, on the one hand, increases, reaching a value of $\approx$2.13 g/cm^3, and, on the other hand, the zone with a material density higher than that of the starting HE decreases.

Similar regularities in the evolution of density profiles in the case of detonation failure and during the transitional regime are observed for the RDX based HE (Fig. 8).

DISCUSSION OF RESULTS

The experimental curves of $\rho(x)$ for different HEs have several characteristic regions: a zone of undisturbed HE, a zone of compressed material, and a zone of abruptly decreased density. Behind the SW front there is a compressed material layer with a width of few millimeters and, as noted above, in the case of detonation failure, the width of this layer increases in the process of explosive transformation. In this case, the density in this region practically does not vary (see Figs. 7 and 8). Behind this region there is a zone in which the material density decreases sharply, perhaps due to the formation of reaction products. The degree of the HE decomposition cannot be determined because unreacted explosive is also present in the indicated region.

The dimensions of the region of the HE compressed behind the SW front depends on the chemical decomposition rate, which is determined by the initial SW intensity. At higher intensities, the decomposition proceeds earlier and faster and the zone of dispersion of the products is closer to the SW front. Figure 9 gives dependences that reflect the change in the dimension of the compression region behind the front in the case of detonation failure for HMX and RDX based HEs. From the figure it is evident that the compressed material region increases with time (shaded area).

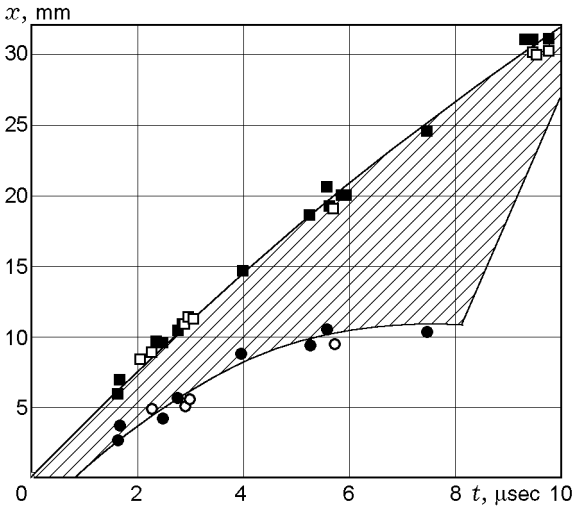

Fig. 9. Evolution of the material compression phase behind the SW front in the case of detonation failure for HMX based HE (filled points) and RDX based HE (open points): points ■ and □ refer to the SW front and points • and ○ refer to the end of the compression phase.

As the initiating SW pressure increased to $\approx$5.5 GPa for the HMX based HE and to $\approx$4.7 GPa for the RDX based HE, a transitional regime of the explosive transformation was detected in the experiment. With close maximum pressures in the loading SW, the depth of shock initiation in the HMX and RDX based HEs are different, which is due to different shock-wave sensitivities of these explosive compositions.

In transition from the initiating SW to detonation, the flow behind the front undergoes some changes. Figure 10 gives curves that reflect changes in the dimensions of the compressed layer behind the front for initiation of detonation of the HMX and RDX based HEs. The arrangement of the experimental points in the figure indicates that the compressed material region for the HMX based HE decreases with time and that for the RDX based HE does not change (the experimental points corresponding to the end of the compression phase are almost parallel to the position of the SW front). This is a distinctive feature of the development of an explosive transformation that does not become a detonation.

In addition, the material density behind the front of an initiating SW that becomes detonation increases with time and has an absolute value higher than that in the case of detonation failure.

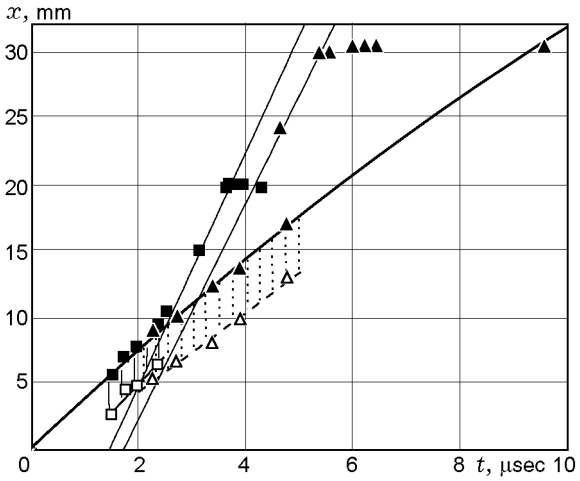

Fig. 10. Evolution of the material compression phase behind the SW front in the case of detonation failure for the HMX based HE (points ■ and □) and RDX based HE (▲ and △): points ■ and ▲ refer to SW and DW fronts; points □ and △ refer to the end of the compression phase.

CONCLUSIONS

Processing of the radiographs yielded dependences $\rho(x)$ that consist of several characteristic regions: the starting unloaded HE; the compressed material behind the SW front; and a zone of sharply decreased density.

The evolution of the density profile behind the front of a divergent initiating SW that becomes or does not become detonation has the following distinctive features.

In the case where the SW does not become a detonation:

- The density profile behind the SW front has a characteristic feature — a segment on which the density of the compressed material is constant;
- As the wave front propagates into the depth of the sample, the dimension of the compressed material layer increases;
- The material density behind the SW front does not increase.

These features of the evolution of the density profile occur in the case of loading by a divergent SW with the following pressure amplitudes: $p \lesssim 4.0$ GPa for the HMX based HE and $p \lesssim 3.2$ GPa for the RDX based HE.

In the case where the SW becomes a detonation:

- The density profile behind the SW does not have a distinct segment of compressed material at constant density;
- As the SW front propagates into the depth of the sample, the dimension of the compressed layer does not increase;
- The density behind the initiating SW front increases up to formation of a stationary DW.

These features in the evolution of the density profile take place for loading by a divergent SW with the following pressure amplitudes: $p \gtrsim 5.5$ GPa for the HMX based HE and $p \gtrsim 4.7$ GPa for the RDX based HE.

A large body of new quantitative data will make it possible to assess the use of different models for the explosive transformation kinetics in two-dimensional calculations and to refine the equations of state for HEs, explosion products, and their mixture for the purpose of constructing a physically more justified model of shock initiation in heterogeneous explosives.

REFERENCES

1. V. A. Komrachkov, A. D. Kovtun, and Yu. M. Makarov, "Use of pulsed radiography in studies of shock-wave initiation of TATB," *Combust. Expl. Shock Waves*, **35**, No. 2, 198–202 (1999).
2. V. A. Komrachkov, K. N. Panov, and T. I. Frolova, "Determination of the material density behind the front of an initiating shock wave in TATB based explosives using flash radiography," in: *Chemical Physics of Combustion and Detonation*, 12th Workshop on Combustion and Explosion, Part II, Inst. of Problems of Chemical Physics, Chernogolovka (2000), pp. 141–144.
3. R. Schall. "Untersuchungen an Detonationsstoβwellen in Leichtmetallen zur Bestimmung der Zustandsgleichung der Metalle," *Z. Angew. Phys.*, **II**, No. 6 (1950).
4. P. I. Zubkov G. N. Kulipanov, L. A. Luk'yanchikov, et al., "Measurements of the material density behind shock and detonation waves using synchrotron radiation," in: *III Khariton Scientific Readings*, Proc. of Int. Conf., Inst. of Exp. Phys., Sarov (2001), pp. 306–311.
5. P. I. Zubkov, G. N. Kulipanov, L. A. Luk'yanchikov, et al., "Observation of transients in low-density HE using synchrotron radiation," in: *V Khariton Scientific Readings*, Proc. of Int. Conf., Inst. of Exp. Phys., Sarov (2003), pp. 204–208.
6. J. D. Zumbro, K. J. Adams, K. R. Alrick, et al., "Proton radiography of the detonation front in HE systems," in: *11th Int. Symp. on Detonation*, Colorado (1998), pp. 54.
7. C. L. Mader, J. D. Zumbro, and E. N Ferm, "Proton radiographic and numerical modeling of colliding, diverging PBX-9502 detonations," in: *12th Int. Symp. on Detonation*, San Diego, California (2002), p. 1040.
8. J. B. Ramsay and A. Popolato, "Analysis of shock initiation of detonation in liquid explosives," in: *4th Int. Symp. on Detonation*, Washington (1965), pp. 233–238.